Title

Photolithography-free laser-patterned HF acid-resistant chromium-polyimide mask for rapid fabrication of microfluidic systems in glass

Journal

Journal of Micromechanics and Microengineering, 27(1)

ISSN

0960-1317

Authors

Zamuruyev, Konstantin O
Zrodnikov, Yuriy
Davis, Cristina E

Publication Date

2017

DOI

10.1088/0960-1317/27/1/015010

Peer reviewed

HHS Public Access

Author manuscript

J Micromech Microeng. Author manuscript; available in PMC 2018 January 01.

Published in final edited form as:

J Micromech Microeng. 2017 January ; 27(1): . doi:10.1088/0960-1317/27/1/015010.

PHOTOLITHOGRAPHY-FREE LASER-PATTERNED HF ACID-RESISTANT CHROMIUM-POLYIMIDE MASK FOR RAPID FABRICATION OF MICROFLUIDIC SYSTEMS IN GLASS

Konstantin O. Zamuruyev, **Yuriy Zrodnikov**, and **Cristina E. Davis***

Department of Mechanical and Aerospace Engineering, One Shields Avenue, University of California, Davis, Davis CA 95616, USA

Abstract

Excellent chemical and physical properties of glass, over a range of operating conditions, make it a preferred material for chemical detection systems in analytical chemistry, biology, and the environmental sciences. However, it is often compromised with SU8, PDMS, or Parylene materials due to the sophisticated mask preparation requirements for wet etching of glass. Here, we report our efforts toward developing a photolithography-free laser-patterned hydrofluoric acid-resistant chromium-polyimide tape mask for rapid prototyping of microfluidic systems in glass. The patterns are defined in masking layer with a diode-pumped solid-state laser. Minimum feature size is limited to the diameter of the laser beam, 30 μm; minimum spacing between features is limited by the thermal shrinkage and adhesive contact of the polyimide tape to 40 μm. The patterned glass substrates are etched in 49% hydrofluoric acid at ambient temperature with soft agitation (in time increments, up to 60 min duration). In spite of the simplicity, our method demonstrates comparable results to the other current more sophisticated masking methods in terms of the etched depth (up to 300 μm in borosilicate glass), feature under etch ratio in isotropic etch (~1.36), and low mask hole density. The method demonstrates high yield and reliability. To our knowledge, this method is the first proposed technique for rapid prototyping of microfluidic systems in glass with such high performance parameters. The proposed method of fabrication can potentially be implemented in research institutions without access to a standard clean-room facility.

1. INTRODUCTION

The physical and chemical properties of glass as well as its compatibility with common microfabrication processes make it advantageous material for numerous MEMS and bio-chip applications. Due to its high chemical resistance properties, glass is especially suited for microfluidic devices used for bioanalysis, mass spectrometry [1, 2], microflow cells for single molecule handling of DNA [3], and micro polymerase chain reaction (PCR) devices for DNA amplification [4]. High optical transparency of glass makes it useful for opto-electric devices [5, 6] and bioanalytical detection systems with optical detection [7–9]. High electric insulation properties of glass make it useful for applications in pressure sensors,

*Correspondence: cedavis@ucdavis.edu.

accelerometers, and RF-MEMS devices [10, 11]. The glass coefficient of thermal expansion is low and similar to that of silicon, making it useful for thermal compensation in many micro-devices [12].

Glass material is compatible with a number of fabrication methods. Mechanical machining with abrasive, drilling, or laser-based processes is commonly used for individual deep cavities and through-holes when surface roughness is not critical. Dry etching [13, 14] is used for wafer level processing when high aspect ratio is required and a slow etch rate with poor smoothness is tolerated. Wet etching in hydrofluoric (HF) acid solution is often preferred due to the high etch rate, smoothness of the etched surface, and compatibility with batch fabrication processes. Fabricated glass microdevices are easily vacuum packaged with anodic bonding to silicon or with fusion bonding to glass.

Currently, there are three major masking methods used for wet etching of glass in HF acid: metal or silicon-based hard masks, photoresist masks, and combination of a hard mask layer with a photoresist layer on top of it.

Bien et al. [15] demonstrated a 300 μm deep etch in aluminosilicate glass (Corning 1737) with the use of a combinational hard mask of polished polysilicon layer with a thick SU-8 layer. Steingoetter and Fouckhardt [16] presented a stress-reduced sputter-deposited chromium hard mask used over fused silica glass with a resulting etch depth up to 104 μm after 7 h. Ong et al. [17] considered optimization of the PECVD amorphous silicon mask and demonstrated a glass etch up to 150 μm. Zhu et al. [5] compared the use of a Au/Cr metal mask and LPCVD deposited poly-Si, amorphous silicon, and silicon nitride masks on fused silica glass, achieving a maximum depth of 100 μm. Although metal-based or silicon-based hard masks show excellent adhesion with the glass substrate and high resistance to HF acid solution, high level of pinholes and notch defects on the edge of the etched geometries are the primary reasons for failure [18]. Increasing the thickness of the hard mask helps to reduce the number of pinhole defects but introduces the problem of residual stress in the mask [17, 19]. The thickness of the mask is limited by the tensile stress level in the deposited mask material, and thus process optimization, annealing, or other approaches are required.

The use of a hard mask with a photoresist layer on top of it has been demonstrated to be a more successful masking method for deep wet etching of glass and fused silica substrates. Bu et al. [20] used a multilayer Cr/Au/Cr/Au metal mask in combination with thick SPR220-7 photoresist to etch 300 μm deep microfluidic components for a micro-peristaltic pump. Iliescu et al. [21] used a 1 μm thick Cr/Au masking layer covered with a hard-baked photoresist layer for a through etch of a 500 μm thick Pyrex® glass wafer, which had been annealed for a higher etch rate. Ceyssens and Puers [22] developed a stress-optimized molybdenum mask layer with a thick SPR220-7 photoresist layer that survived 3.5 h duration etch and resulting in 1.2 mm deep features. Jin et al. [23] completed a 20 h duration etch; 525 μm deep etch of fused silica with 430 nm thick Cr/Au hard mask layer and 5.2 μm thick AZ4330 positive photoresist.

The application of AZ5214e photoresist mask alone on glass and fused silica was proposed by Grosse et al. [9], and AZ4620 photoresist by Lin et al. [24]. The reported mask survival period in HF acid is ~30 min with resulting depths of 35 μm in fused silica. Although a photoresist mask on glass excludes application of metal mask interlayer, photoresist mask preparation is still sophisticated and prone to failure. It requires a thorough surface cleaning, ramped baking cycles to minimize thermal mismatch between photoresist and the glass surface, and optimized UV exposure limits.

The creation of photoresist mask on glass [9, 24] proposed in 2001 was never confirmed by others. Instead, two other research groups reported on instant photoresist mask failure within the first minute after submersion into HF solution [5, 15]. Bien et al. [15] tried to develop a photoresist mask using S1813 and SU-8 photoresists and found that the photoresist mask peels off instantly when placed into HF acid solution. Zhu et al. [5] also attempted to prepare a reliable photoresist mask using AZ3312, AZ4620, and AZ5214 photoresists with different thicknesses. They reported that the photoresist masks peeled off in 1 min after emersion into an HF acid bath.

Therefore, in spite of the time and cost to prepare a combinational mask that has a thick photoresist layer on top of a hard-mask layer, it is still the preferred masking method due to its reliability in wet etching of glass.

In this paper, we report a new glass masking method with a chromium metal layer and adhesive polyimide tape (Kapton® tape) for rapid prototyping of microfluidic systems in glass using wet etching. The method demonstrates a deepest average etch of 298 μm in Schott Borofloat® 33 glass and has a minimum feature resolution of 40 μm due to laser and masking material limitations. It is not our intention to make a direct comparison of this method to metal-photoresist mask due to its limitations in resolution and maximum depth. The proposed method cannot fully substitute the traditional masking method with a metal layer and thick hard-baked photoresist layer; but it can be a useful fabrication technique for rapid prototyping of microfluidic systems. The method offers advantages of shorter fabrication time, easiness, and cost. The photolithography-free method allows rapid changes in the design for microfluidic system optimization.

Several examples of fabricated microsystems are demonstrated in figure 1. A variety of shapes and sizes are available for liquid and gas phase chemical detection applications. Void-free bonding of the fabricated chips with either anodic or thermal fusion bonding demonstrated that no material was etched in the mask protected regions. A simple microscope inspection and fill of the microchannels with fluid showed no signs of defects. No entrapped air cavities were visible. No surface defects that created a capillary passage network for fluid leaks were noticed. Neighboring parallel channels showed no common interconnects (leakages) or fluid dispersion into bond interface by capillary action. The ink-filled microchannels in figure 1 (c) show no leakage or closed channel defects. The proposed method can be applied to individual microchip-sized glass substrate or to wafer level microfabrication processes. A 4 inch wafer containing 6 microfluidic chips is laser-patterned in 22 min, etched for 15 min in 49% HF acid, and anodically bonded to silicon wafer in 3 h. The bonded wafers containing microfluidic patterns are cut into individual chips with a

dicing saw (Disco DAD 321, Japan). The whole microfabrication process, from laser patterning to glass thermal fusion bonding, took under 4 hours. It is comparable or shorter than a preparation of an HF resistant photoresist mask alone on a metal coated glass surface.

2. METHODS

2.1 Glass substrates and mask preparation

The experiments were performed with 50×50×0.8 mm^3 borosilicate (Borofloat® 33 by Schott Co.) glass slides. This type of glass is distinguished for outstanding thermal resistance to rapid temperature changes, exceptional transparency, high chemical durability, and excellent mechanical strength. The slides were cleaned in 4:1 Piranha solution (H_2SO_4/H_2O_2) and sputter-coated with a 180 ± 28 nm chromium layer. Polyimide tape with adhesive side (Kapton®) was applied on the chrome coated surface of the slide. Total tape thickness was 50 μm; it included polyimide tape layer and adhesive silicone layer. The tape was gradually applied from one side of the slide with soft plastic spatula (12.5 mm wide) to avoid air bubbles and ensure good contact of adhesive.

In order to see the effect of each masking material individually, four groups of substrates were prepared. The sole effect of chromium mask was verified with 8 glass slides with chromium metallized layer only - no adhesive polyimide tape. The sole effect of adhesive polyimide tape mask was verified with 6 glass slides with adhesive polyimide tape applied on clean glass surface – with no chromium metal interlayer. The effect of combination of two masking layers was verified with 18 glass slides with chromium metal layer and adhesive polyimide tape on top of it. The effect of temperature on mask stability was verified with 6 glass slides that had chromium metal layer and adhesive polyimide tape. This group of substrates was baked at 160 °C in vacuum oven for the period of 120 min or longer before laser patterning step.

2.2 Defining micropatterns with laser

The geometries were patterned with a commercial diode-pumped solid-state laser (Samurai UV Marking/Micromachining System, model 3530-30; wavelength 355 nm UV, equipped with telecentric lens, F=103 mm; DPSS Lasers, Santa Clara USA). The laser parameters were set at 1.5 Watt, 70 kHz frequency, and 100 mm/sec scan speed with path repetition of 100. With these power parameters and installed optical lens, the minimum feature size was limited to the diameter of the laser beam (30 μm) while the minimum spacing between features was limited by the thermal shrinkage and adhesive contact of the Kapton® tape to 40 μm. The inner area of the geometries with dimensions larger than the laser beam diameter was filled with multiple laser passes with a 10 μm space increment from pass-to-pass. The minimum power input to define geometries was preferred to avoid distortion of fine features and glass cracking.

2.3 Mask for etch optimization

The mask for etch optimization consisted of 12 regions containing straight lines and some chess-style squares (figure 2). Each region contained 19 lines of the same width but distributed in spacing. The width of the lines increased from 35 μm in region one, to 200 μm

in region twelve, which allowed us to investigate the dependence of the etch rate on geometry opening width. In each region, the spacing width between lines increased from 40 μm to 373 μm. The laser settings, mask pattern, and etching conditions were kept the same for the four masking methods except that features spacings, in each region, were increased to range from 40 μm to 1500 μm for the chromium-polyimide baked mask because of the much longer etch period. The variable spacing allowed us to determine the minimum features spacing (highest density) as a function of the masking material and etched depth. The mask pattern was composed in CAD and imported into WinLase® commercial laser marking software (Lanmark Controls Inc., USA). The actual features dimensions differed from those assigned in the CAD file when patterned in the masking layer. The mask openings were wider and the spacings were narrower by the diameter of the laser beam. The actual mask dimensions were confirmed for each masking method with a profilometer (DektakXT™, Bruker Corp.).

2.4 Glass etching in 49% HF acid

The laser-patterned substrates were cleaned from debris with a short DI water rinse and 1 min DI water sonication bath. The prepared substrates were etched in 49% hydrofluoric acid with soft agitation. A preliminary experiment was done before the main study to determine the maximum etch time period for each masking method. Three glass substrates per masking method were kept in the acid bath until noticeable mask defects occurred. The mask survival period was 6, 4, 18, and 60 min for each group respectively. The number of prepared glass substrates in each group corresponded to the maximum etch period divided by specified time increment; 1 min increment for short etches and 10 min increment for 60 min etch.

To determine the etch rate and confirm the maximum time period for each masking method, the glass substrates of one group were placed into the acid bath and taken out at one min increments until noticeable defects occur in the mask. All etching was done in a fume hood equipped for acid wet etching with an operator wearing acid resistant personal chemical protection.

2.5 Mask quality characterization

The quality of the etched features was characterized with a profilometer (DektakXT™, Bruker Corp.). For each masking method, three scans were made at different positions across each region for each etch period (min). The measured depths of the etched features were used to evaluate the etch rate and its dependence on mask opening width. The measured widths of the etched features were used to evaluate the under etch ratio and minimum feature spacing. All profilometer data were saved as .CSV files for the subsequent data processing steps. Three profilometer scans over 19 features in each region contained 57 profiles for evaluating depth and etch rate, width and under etch ratio. The only exception was the adhesive polyimide mask that showed strong dependence of the under etch ratio on features spacing; only 3 feature profiles were available for evaluating etch parameters.

The depths, widths, and under etch ratio were evaluated using MATLAB® software. The three profilometer data files for each masking method, region, and etch time were aligned at the middle of the first etched feature, averaged over the 3 scans, and processed into plots.

The width of each etched line was evaluated with a threshold value set below the level of the top flat surface. The 2 data points at the specified threshold defined the upper corners (width) of the etched feature. The under etch ratio was evaluated based on the measured mask opening width before etch and feature width after etch. To be conservative in reporting the etched depth of the isotropic profile, the number of data points corresponding to the width of the feature was divided into three parts; the average depth value of the points in the middle part was used to evaluate the feature depth.

The mask damage was evaluated with two parameters: the under etch ratio of thin regions separating two etched cavities and the amount of pinhole defects in the areas protected with the mask.

Any separating planar region, in two out of three scans, that had height equal to or lower than 500 nm below the original unetched planar surface of the substrate was considered to be damaged in the etch. Variable spacing width of the separating regions allowed us to determine the minimum width for the separating region between two etched cavities as a function of the etched depth.

The maximum survival time of the mask was determined when the widest separating region (373 μm, 1500 μm in case of a 60 min long etch) showed early signs of mask saturation such as slight change in mask color due to capillary HF acid penetration into the adhesive interlayer. This time point was conservative to stop etch before masked glass surface was damaged. Larger mask widths were not considered because they might be beyond the useful size range for microscale designs.

The roughness of the substrate due to mask pinhole defects was estimated from optical and scanning electron microscope (SEM) images. The area and depth of pinholes were estimated with ImageJ, an open platform for scientific image analysis. The depth of pinhole defects was estimated based on their area. Since most pinholes had circular shape and were assumed to initiate from negligible initial size, we estimated their depth as equal to the radius of their area. Their depth was also confirmed with profilometer measurements of the surface roughness. Five profilometer scans, 10 mm long each, were made across the blank field of each substrate to confirm the results from the image analysis. The percent fraction of the surface affected with pinholes was estimated with the ratio of the total area of pinhole defects to the total area of the image.

All computer processed results were confirmed with SEM images and measurements.

3. RESULTS AND DISCUSSION

The purpose for this work was to introduce and characterize a novel photolithography-free masking method for wet etching of glass microchips. The reported values characterize the masking method during its stable time range before fatal mask delamination or severe surface defects occur. A series of etches were performed using the etch characterization pattern (figure 2). We refrained from using solely the time basis and preferred to characterize the mask in terms of etched depth. Etch time can be affected by the size of features, bath temperature, and agitation. Large features provide more access for acid circulation and

byproducts removal and thus are etched at a faster rate than smaller features (figure 6 (a)). A temperature increase of a few degrees can speed up the etch process significantly. Active agitation or sonication has a huge effect on the etch rate too. Thus, operating with the final etched depth would be a more accurate measure for other researchers to use this proposed method for their projects.

In order to investigate the effect of each masking component (chromium metal layer, adhesive polyimide tape, and effect of adhesive mask bake) four groups of substrates were processed. It was experimentally observed that reported mask stability was not due to the quality of a single component but due to their combination. It was not high quality Chromium metal layer that held the etch, nor was it the polyimide tape alone, and neither was it the hard-baked adhesive glue to the glass surface, but it was their combination. Chromium metal layer increased stability of adhesive polyimide tape on the substrate while polyimide tape effectively covered all pinholes and crack defects in the metal layer. Baking this combinational mask before laser patterning further improved mask stability.

Scanning electron microscope (SEM) images (figure 3) demonstrate the quality of the etched microstructures in glass. The wiggly serpentine microchannel has accurate edges and shape. Based on the profilometer and SEM measurements, the average under etch ratio of the etched geometries is 1.36. Figure 3 (b) demonstrates the sharpness of the etched features. The straight wall, separating two microfluidic channels, has a minimum under etch and straight sharp upper corner. The volcanic-like roughness of the etched surface has two possible origins: due to pulsating nature of the laser that produces mask edge roughness or due to aggressive glass etching in the concentrated HF solution. The initial roughness of the mask edge can be reduced with better optimization of the laser settings, reduced power and increased pulsating frequency. Also, alternatively off shifting the position of the laser pulses between repetitive paths may minimize the edge roughness of the mask. Another reason for roughness of the etched features is the presence of Al_2O_3, CaO, MgO compounds in borosilicate glass that form insoluble products (CaF_2, MgF_2 or AlF_3) with HF acid [25]. These insoluble in HF acid products may create local masking and increase the roughness of the etched microstructures. Iliescu et al. [26] proposed addition of HCl to HF acid (10:1 HF (49%) / HCl (37%) to dissolve these products for a smoother etch.

Figure 4 shows an SEM image of the cross section of the etched profiles and cavity depth development at different time points of etch. Figure 4 (b) compares the depth and the under etched distance for the three masking methods. Although adhesive polyimide tape mask on glass can be useful for shallow etches, the wide under etched distance makes it unsuitable for applications where sharp well defined edge features are required. Chromium metal hard mask demonstrates minimum under etch for depth up to 45 μm but fails in longer acid etch. Addition of adhesive polyimide mask over the chromium layer allows for nearly twice as deep etch with no compromise in under etch ratio and is effective for masking most pinhole defects in the chromium layer. Baking chromium-polyimide mask in vacuum oven before laser patterning step, extends its survival time and results in depth up to 300 μm with no compromise in the under etch ratio (figure 4 (c)). Baking chromium-polyimide mask before laser patterning step reduces the stress in the adhesive silicone layer and improves its

adhesion with the chromium coated surface. Baking polyimide mask applied on clean glass surface has no improvement effect on mask stability.

We demonstrate the concept of feature density with the etch of multiple line cavities placed to one another at decreasing spacing. Figure 5 (b) shows overlaid profilometer scans of the etched features for the three masking methods. A set of 98 μm wide lines has variable mask spacing from 300 to 33 μm. The required mask spacing distance increases with the etched depth for all masking methods due to isotropic under etch. As the depth of the etched features increases, the masking material is under etched and feature spacing is ruined. The polyimide adhesive tape mask on glass fails quickly when the spacing between etched features is <180 μm. The acid penetrates under the mask and etches away bulk material separating the two cavities. Chromium and chromium-polyimide masks allow deep microfeatures at minimum spacing. Addition of adhesive polyimide tape over the chromium metal layer allows nearly twice the etched depth with no compromise in minimum feature spacing.

Figure 6 compares 4 masking methods in terms of the etch rate, under etch ratio, maximum etch period and ratio of minimum features spacing per etched depth. Figure 6 (a) demonstrates the dependence of the etch rate on the initial mask opening width of the feature. In general, wider geometries are etched at faster rates. The chromium metal hard mask demonstrates little dependence of the etch rate on the mask opening width while masks with adhesive polyimide tape show strong dependence for geometries with mask opening width < 60 μm. The strong dependence of etch rate on narrow mask opening width for adhesive polyimide masks may be due to the presence of adhesive layer (glue) between glass and polyimide. The laser ablated parts of the glue (burned flake particles) may fill the narrow gaps and prevent acid access to the etched cavity. Longer DI water sonication bath or more optimized laser settings may reduce this dependence. The etch rate approaches a constant value as the width of the features increases. The overall decrease in the etch rate for the chromium-polyimide tape mask in comparison to the chromium mask may be due to the increased thickness of the mask (50 μm) and not fully optimized laser settings. The laser settings are intentionally kept constant for all 4 masking methods for direct comparison of mask stability in etch (eliminate dependence on laser patterning) otherwise the laser settings should be optimized for a specific masking material.

Glass etching in HF acid-containing solutions is an isotropic process with a minimum under etch ratio of 1. Thus, the theoretical limit of aspect ratio, assuming negligible mask opening width, is limited to 2; i.e. the etched feature is twice as wide as it is deep. But practically, the etched feature is wider due to initial mask opening width and mask under etch ratio greater than 1. Based on our measurements of etched features to different depths, the average under etch ratio is 1.37 for chromium-adhesive polyimide tape mask.. Figure 6 (b) compares the masking methods in terms of the geometry under etch ratio and demonstrates how close one can place microstructures that are to be etched to a certain depth. The isotropic under etch ratio is evaluated with measurements of width and depth of the etched features as described in the Methods section. The under etch ratio is defined as the half difference between final width of the etched feature and initial width of the mask opening divided by the depth of the etched feature. Chromium and chromium-polyimide masking methods demonstrate a low

under etch ratio (~1.36) and allow for a relatively high density of etched features. The adhesive polyimide tape mask on glass (no Chromium layer) demonstrates a high dependence of under etch ratio on the feature spacing. Any features that are placed closer to each other than 180 μm fail to survive the 4 min (30 μm deep) etch; the mask is lifted up and peels off. The under etch ratio decreases as the spacing between features increases. The error bars in figure 6 (a, b) correspond to one standard deviation above and one standard deviation below the average value. The lines connecting the data points are interpolated and serve only for visual inspection.

Figure 6 (c) compares 4 masking methods in terms of the maximum mask survival time period, features etched depth, mask under etch ratio, and ratio of minimum features spacing per etched depth. The maximum etch time period specifies the duration of etch before noticeable defects occur in the mask and etched features. The mask survival period, etched depth, and under etch ratio may depend on the size of the geometries, their spacings, and bath agitation. In general etch rate decreases with etch duration and has high dependence on agitation. The values are average, based on multiple measurements of etched features with different mask opening and spacing widths. The ratio of minimum spacing per etched depth is an average value per each masking method based on measured under etch ratio and direct experimental observations. The minimum spacing may depend not solely on under etch ratio but also on the minimum mask adhesion area for masks that involve application of adhesive polyimide layer. The experimental results show that this dependence is strong only when adhesive polyimide layer is applied on clean glass surface. The minimum spacing between etched features mainly depends on the under etch ratio for chromium or chromium-polyimide masks.

Figure 7 compares the quality of the etched features for the 4 masking methods. The SEM images show not only under etched regions of the etched features but pinhole and edge defects. The chromium hard mask (figure 7 (a, b)) shows a high number of pinhole defects. The defects are especially harmful when located at the edges of the etched features. The chromium mask is also very susceptible to scratches introduced while handling the substrate. The adhesive polyimide mask is simple to apply but shows severely washed away feature edges that lack sharp corners (figure 7 (c, d)). The polyimide tape mask applied on a clean glass surface can withstand only a shallow etch, up to 30 μm versus 45 μm for the chromium mask, and 80 μm for the chromium-polyimide mask. The chromium-polyimide mask (figure 7 (e–h)) demonstrates not only the deepest etch but also the highest quality against pinhole and scratch defects. Comparing pinhole density of the 4 masks, we find that polyimide covered substrates have minor pinhole defects only in the 60 min long etch and practically no pinhole defects in shorter etches.

Figure 8 shows some representative images of pinhole defects for chromium masked substrate etched 6 min in 49% HF acid and chromium-polyimide masked substrate etched 60 min in 49% HF acid. The images clearly relate the benefits of using adhesive polyimide tape in terms of maximum etched depth (survival time) and mask quality. The presence of pinholes in the deposited Chromium layer was not a significant problem for the proposed combinational mask of sputtered Chromium with adhesive polyimide tape. Spatially dispersed from each other groups of pinholes and individual pinholes were observed.

Adhesive polyimide tape closed affectively the pinhole defects such that they were hardly noticed in the considered time range (up to 250 μm deep, ~ 40 min long). The pinhole defects were more apparent at longer etch periods (60 min) as shown in figure 8. Figure 8 (c) provides a summary for the analysis of surface pinhole defects. Although, the analysis was done with multiple images representing the surface areas that were affected with pinholes, the use of error bars to show deviations from the average was avoided because distribution density of pinholes on the substrate surface had localized nature and separate images were not representative for the whole substrate surface area.

In this work the optimization of metal layer quality was not considered. For all cases the chromium layer was sputter-coated in a single batch. Therefore, the quality of the chromium layer on glass slides should be the same for all chromium layer masked and chromium-polyimide masked substrates. The demonstration of chromium mask on glass surface was only for the purpose to show the comparative improvement due to application of adhesive polyimide layer. Better optimization for quality of the chromium layer will improve equally the performance of all masking methods that use chromium layer: chromium mask, chromium-polyimide, and baked chromium-polyimide tape mask.

The presented results characterize masking methods for the deepest (aggressive) etch in 49% HF acid. Shallow and more controlled etches can be done with various concentrations of Buffered Oxide Etchant (BOE) solutions. The proposed mask can withstand several hours-long 6:1 BOE etch but the etched depth is very shallow due to lower etch rate of glass. The mask eventually fails mainly due to the duration of the etch. BOE solution penetrates through adhesive layer of polyimide tape and ruins the mask interface.

4. CONCLUSION

We describe a new glass masking method with: mask stability in terms of maximum etch rate and maximum etched depth; feature density in terms of under etch ratio and minimum feature spacing. The composite chromium-polyimide tape (Kapton® tape) mask demonstrates the best results; 18 min long etch (~80 μm deep features, 1.37 under etch ratio, minimum etched feature aspect ratio of 3.04) and 60 min long etch (~300 μm deep features, 1.36 under etch ratio, minimum etched feature aspect ratio of 3.02) when mask is baked prior to laser patterning step. Due to its resolution and etch depth limitations, the proposed method is not suggested as a full substitute to currently-used methods involving a metal hard mask with thick photoresist. But we find the proposed method to be very useful for rapid manufacturing of gas and liquid microfluidic systems because of its simplicity and reliability. We demonstrated the time benefit of the proposed method with 6 microfluidic chips (figure 1) fabricated on a 4 inch glass wafer in 1 h and anodically bonded in 3 h. It is comparable or quicker than preparation of a reliable metal-photoresist mask alone that requires hours of cleanroom work time. The method demonstrated high repeatability and reliability, more than 60 substrates were prepared and etched in 49% HF acid and only two substrates (masks) failed. In both cases it was evident that the Chromium coated surface was contaminated prior to the metallization step. The use of a laser to define the microfluidic features in the chromium-polyimide tape mask side-steps the costly and time consuming photolithography process. The use of the laser, instead of a shadow mask for

photolithography, also allows rapid layout and size change of microfeatures which is very beneficial for faster microfluidic chip design development and performance optimization. The crack-free nature of wet etching makes this method advantageous over abrasive mechanical machining or laser-based etching processes when fabricated device is exposed to multiple rapid temperature and pressure loadings. Therefore, it can be a useful method for rapid microfabrication of devices where crack-free surface finish is critical.

One further improvement that we can advise to increase the resolution of the pattern is to study the effects of laser focal length point. The referenced laser system allows installation of telecentric lens with different focal point lengths. The one that was available for this work was 103 mm. Experimenting with a lens capable of better laser beam focusing may improve the minimum features size.

The proposed method of fabrication can potentially be implemented in research institutions with no access to a standard clean-room facility. Chromium-coated glass slides can be acquired from a commercial supplier. The laser patterning step does not require a dust-free environment. Glass HF etch can be done in a regular fume hood equipped for wet etching. The bonding step is the only step that requires a particle free environment.

Considering the listed benefits of the proposed photolithography-free laser-patterned HF acid-resistant chromium-polyimide mask and comparable results to current glass masking methods, it can be a useful tool for rapid fabrication of microfluidic systems in glass.

Acknowledgments

Partial support was provided by: the NIH National Center for Advancing Translational Sciences (NCATS) through grant #UL1 TR000002 [CED]; NIH award U01 EB0220003-01 [CED]; NIH award 1P30ES023513-01A1 [CED]; and NSF award #1255915 [CED]. Student support was provided by NIH award T32 HL07013 [KOZ] and NIH award #P42ES004699 [KOZ]. The contents of this manuscript are solely the responsibility of the authors and do not necessarily represent the official views of the funding agencies. The authors are grateful to lab members Sierra Spitulski and Daniel Peirano for assistance with computerized processing of CAD and profilometer data files.

References

1. Koh Y, et al. Bead affinity chromatography in a temperature-controllable microsystem for biomarker detection. Analytical and Bioanalytical Chemistry. 2012; 404(8):2267–2275. [PubMed: 22986986]
2. Saarela V, et al. Glass microfabricated nebulizer chip for mass spectrometry. Lab on a Chip. 2007; 7(5):644–646. [PubMed: 17476387]
3. Rusu C, et al. Direct integration of micromachined pipettes in a flow channel for single DNA molecule study by optical tweezers. Journal of Microelectromechanical Systems. 2001; 10(2):238–246.
4. Obeid PJ, et al. Microfabricated device for DNA and RNA amplification by continuous-flow polymerase chain reaction and reverse transcription-polymerase chain reaction with cycle number selection. Analytical Chemistry. 2003; 75(2):288–295. [PubMed: 12553764]
5. Zhu HX, et al. Characterization of deep wet etching of fused silica glass for single cell and optical sensor deposition. Journal of Micromechanics and Microengineering. 2009; 19(6)
6. Nagarah JM, Wagenaar DA. Ultradeep fused silica glass etching with an HF-resistant photosensitive resist for optical imaging applications. Journal of Micromechanics and Microengineering. 2012; 22(3)
7. Gotz S, Karst U. Recent developments in optical detection methods for microchip separations. Analytical and Bioanalytical Chemistry. 2007; 387(1):183–192. [PubMed: 17031620]

8. Cheng Y, Sugioka K, Midorikawa K. Microfluidic laser embedded in glass by three-dimensional femtosecond laser microprocessing. Optics Letters. 2004; 29(17):2007–2009. [PubMed: 15455762]
9. Grosse A, Grewe M, Fouckhardt H. Deep wet etching of fused silica glass for hollow capillary optical leaky waveguides in microfluidic devices. Journal of Micromechanics and Microengineering. 2001; 11(3):257–262.
10. Park HW, et al. Feed-through capacitance reduction for a micro-resonator with push-pull configuration based on electrical characteristic analysis of resonator with direct drive. Sensors and Actuators a-Physical. 2011; 170(1–2):131–138.
11. Kim JM, et al. Electrostatically driven low-voltage micromechanical RF switches using robust single-crystal silicon actuators. Journal of Micromechanics and Microengineering. 2010; 20(9)
12. Yoo S, et al. Monolithically integrated glass microlens scanner using a thermal reflow process. Journal of Micromechanics and Microengineering. 2013; 23(6)
13. Baram A, Naftali M. Dry etching of deep cavities in Pyrex for MEMS applications using standard lithography. Journal of Micromechanics and Microengineering. 2006; 16(11):2287–2291.
14. Ray T, Zhu HX, Meldrum DR. Deep reactive ion etching of fused silica using a single-coated soft mask layer for bioanalytical applications. Journal of Micromechanics and Microengineering. 2010; 20(9)
15. Bien DCS, et al. Characterization of masking materials for deep glass micromachining. Journal of Micromechanics and Microengineering. 2003; 13(4):S34–S40.
16. Steingoetter I, Fouckhardt H. Deep fused silica wet etching using an Au-free and stress-reduced sputter-deposited Cr hard mask. Journal of Micromechanics and Microengineering. 2005; 15(11): 2130–2135.
17. Ong YY, et al. Process Analysis and Optimization on PECVD Amorphous Silicon on Glass Substrate. International Mems Conference 2006. 2006; 34:812–817.
18. Simpson PC, Woolley AT, Mathies RA. Microfabrication Technology for the Production of Capillary Array Electrophoresis Chips. Biomedical Microdevices. 1998; 1(1):7–25.
19. Iliescu C, Miao JM, Tay FEH. Stress control in masking layers for deep wet micromachining of Pyrex glass. Sensors and Actuators a-Physical. 2005; 117(2):286–292.
20. Bu MQ, et al. A new masking technology for deep glass etching and its microfluidic application. Sensors and Actuators a-Physical. 2004; 115(2–3):476–482.
21. Iliescu C, Tay FEH, Miao JM. Strategies in deep wet etching of Pyrex glass. Sensors and Actuators a-Physical. 2007; 133(2):395–400.
22. Ceyssens F, Puers R. Deep etching of glass wafers using sputtered molybdenum masks. Journal of Micromechanics and Microengineering. 2009; 19(6)
23. Jin JY, et al. Deep wet etching of borosilicate glass and fused silica with dehydrated AZ4330 and a Cr/Au mask. Journal of Micromechanics and Microengineering. 2014; 24(1)
24. Lin CH, et al. A fast prototyping process for fabrication of microfluidic systems on soda-lime glass. Journal of Micromechanics and Microengineering. 2001; 11(6):726–732.
25. Spierings GACM. Wet Chemical Etching of Silicate-Glasses in Hydrofluoric-Acid Based Solutions. Journal of Materials Science. 1993; 28(23):6261–6273.
26. Iliescu C, et al. Characterization of masking layers for deep wet etching of glass in an improved HF/HCl solution. Surface & Coatings Technology. 2005; 198(1–3):314–318.

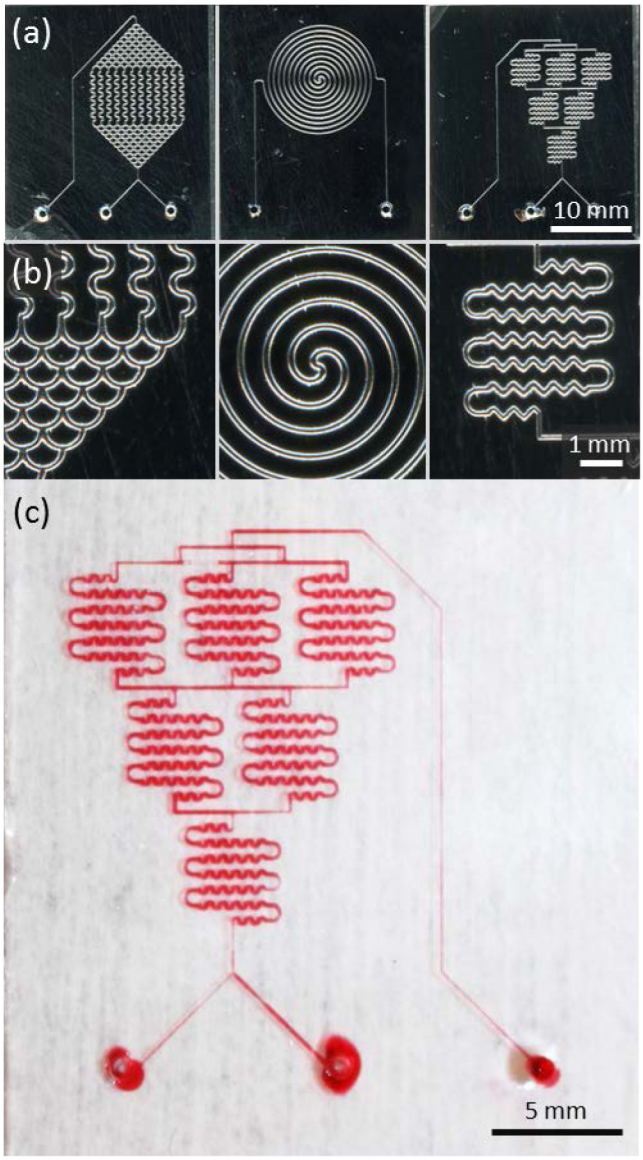

Figure 1.

Fabricated microfluidic devices etched in glass with composite (chrome and polyimide tape) mask. Microchannels with initial mask opening width of 40 μm are etched in 49% HF for 15 min. Etched microchannels are 75 μm deep and 225 μm wide. (a, b) Etched glass wafer is anodically bonded to silicon surface. (c) Surface with etched microchannels is bonded to a plain glass surface in thermal fusion. The wavy microchannels filled with red ink show no leakage or closed channel defects.

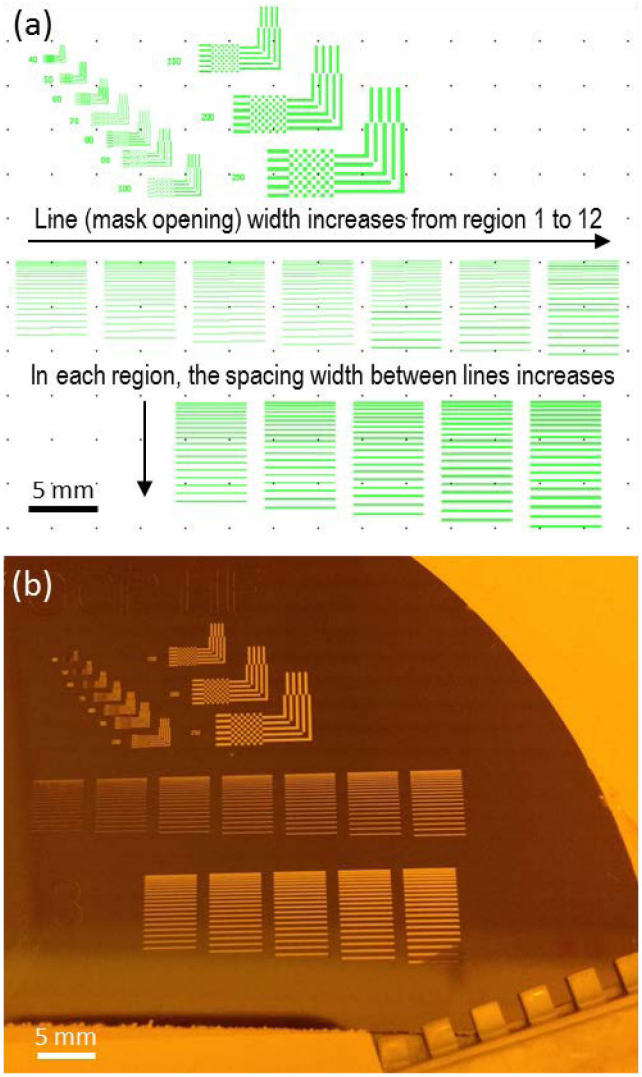

Figure 2.

Mask for etch optimization consists of twelve regions containing straight lines and chess-style squares. Each region contains nineteen lines of the same width but distributed in spacing. The width of the lines increases from 35 μm, in region one, to 200 μm, in region twelve; the spacing width between lines increases from 40 μm to 373 μm in each region.

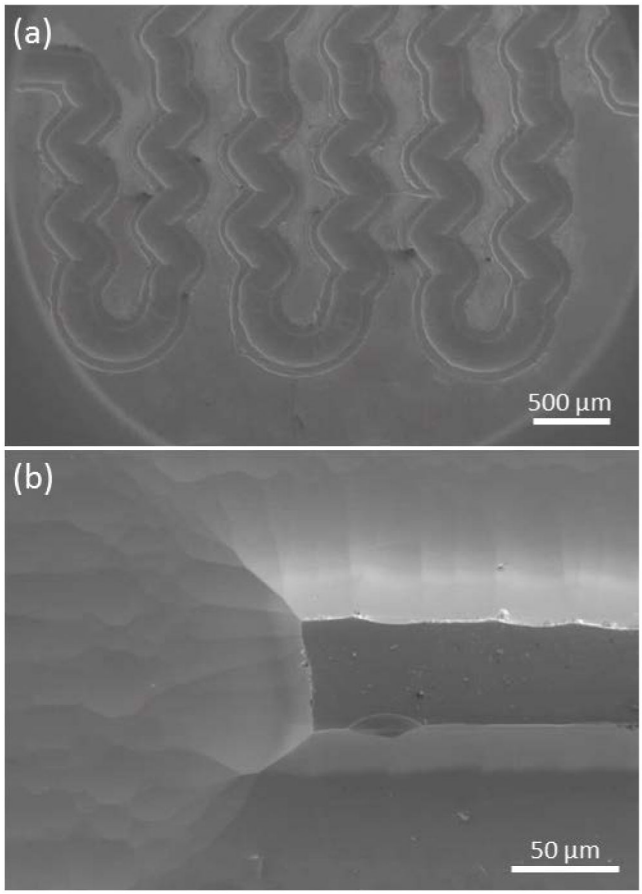

Figure 3.

SEM images of the microstructures etched in 49% HF with composite mask. (a) Wiggly microchannel. Initial mask opening 130 µm, mask spacing 460 µm. Etched depth 90 µm, final microchannel width 374 µm, and spacing width 217 µm. (b) Straight edge wall separating two 80 µm deep microchannels.

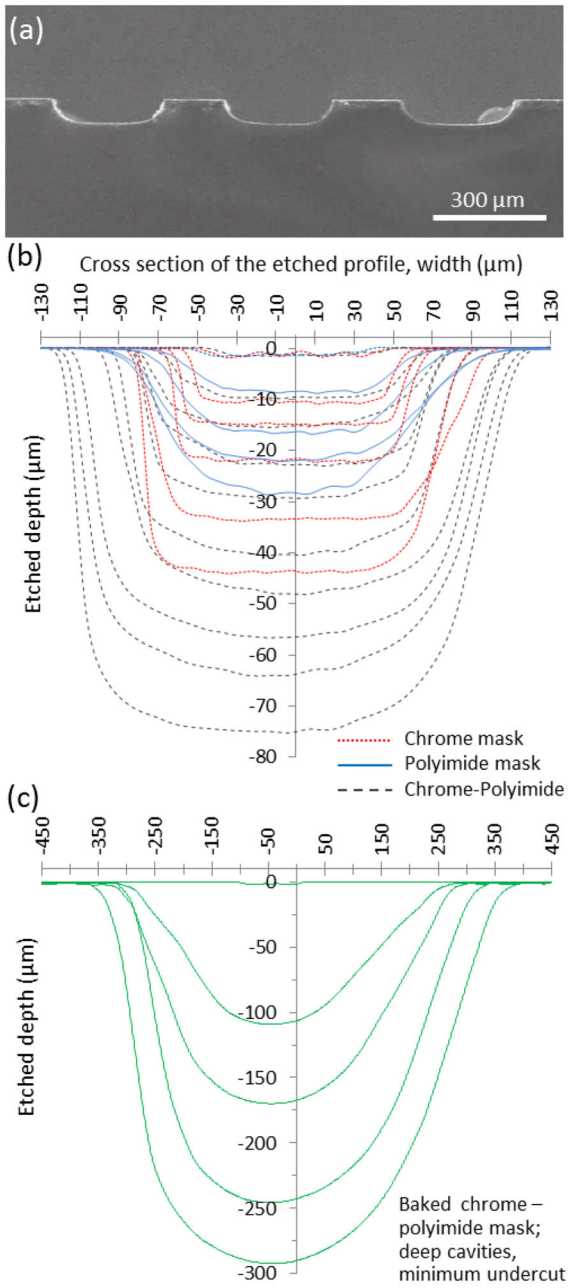

Figure 4.

Depth and under etch ratio. (a) SEM image of cross sectional profile of 75 µm deep lines etched in 49% HF with chromium-polyimide mask. (b, c) Profilometer scan of the etched feature at different time points. Initial mask opening width is ~100 µm. (b) Comparison of mask under etch ration for the three masking methods. (c) Baked chromium-polyimide mask withstands much longer etch with minimal mask undercut ratio.

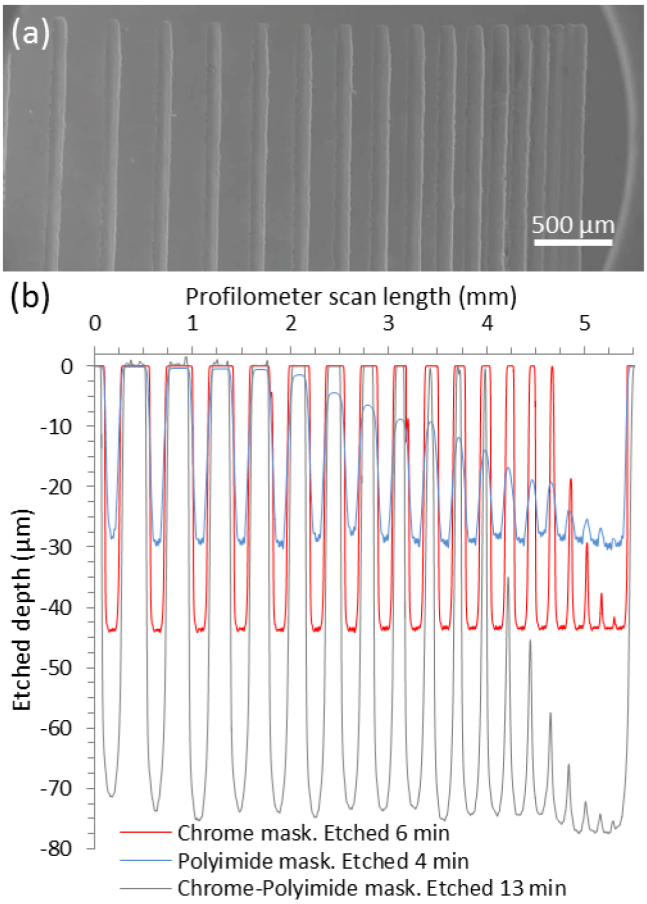

Figure 5.

Feature density: minimum required mask spacing between the etched features. The required spacing increases with the etched depth for all masking methods. All etched geometries have width of 98 µm, while spacing width decreases from 300 µm to 33 µm. The chromium-polyimide mask demonstrates the highest feature density and mask stability for deepest etch. (a) SEM image of the scanned geometries. (b) Overlaid profilometer scans of the etched features for the three masking methods.

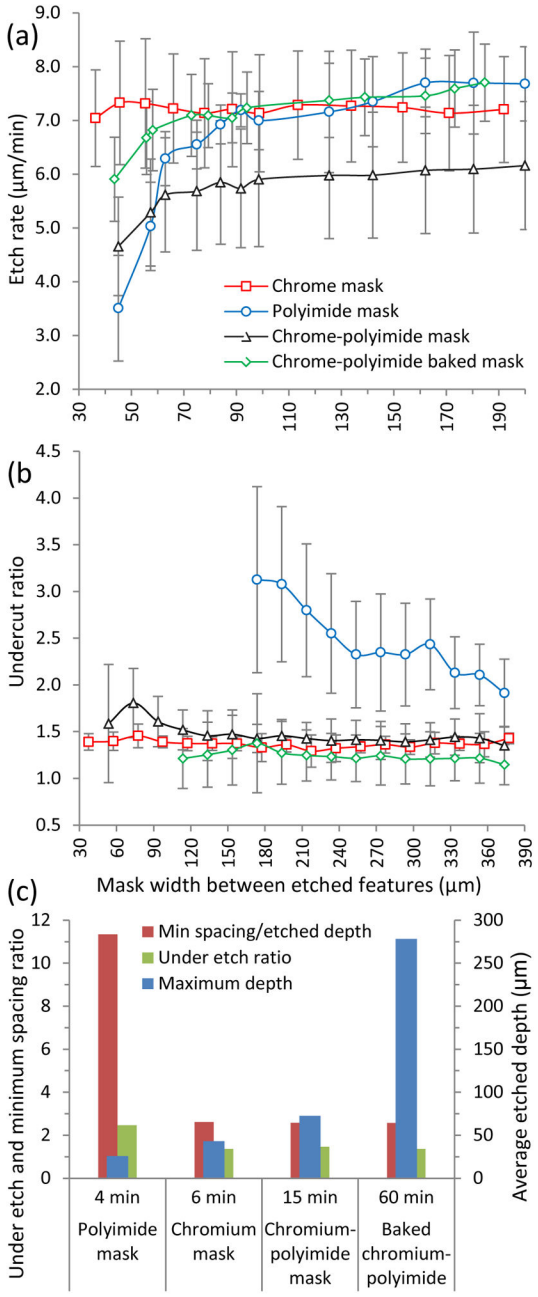

Figure 6.

Comparison of masking methods. (a) Etch rate (µm/min) as a function of mask opening (geometry) width. (b) Mask under etch ratio as a function of mask spacing width between features. (c) Maximum etch time, average depth, under etch ratio, and minimum spacing per etched depth ratio.

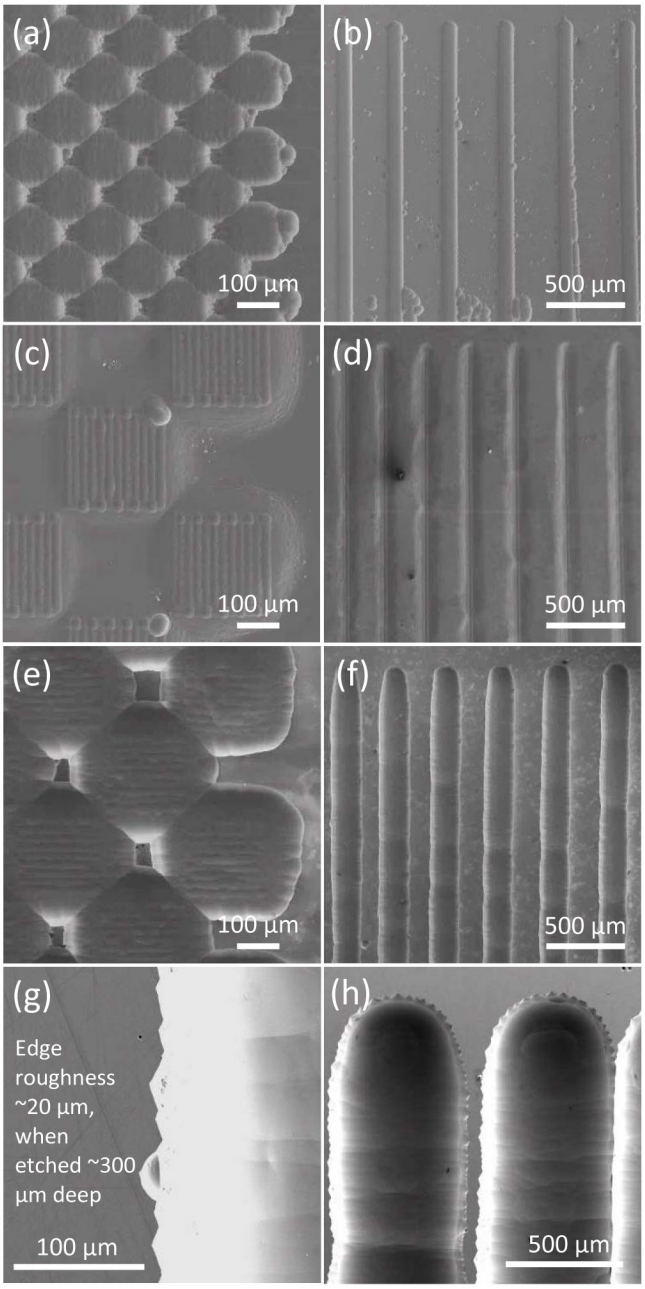

Figure 7.

Comparison of the quality of the etched features for different masking methods. (a, b) Chromium mask; 30 µm deep etch. Initial square size 90 µm and line width 45 µm. (c, d) Polyimide tape mask; 17 µm deep etch. Initial square size 250 µm and line width 57 µm. (e, f) Chromium and polyimide tape mask; 65 µm deep etch. Initial square size 200 µm and line width 57 µm. (g, h) Baked chromium-polyimide mask; 298 µm deep etch. Edge roughness ~ 20 µm, initial line width 48 µm.

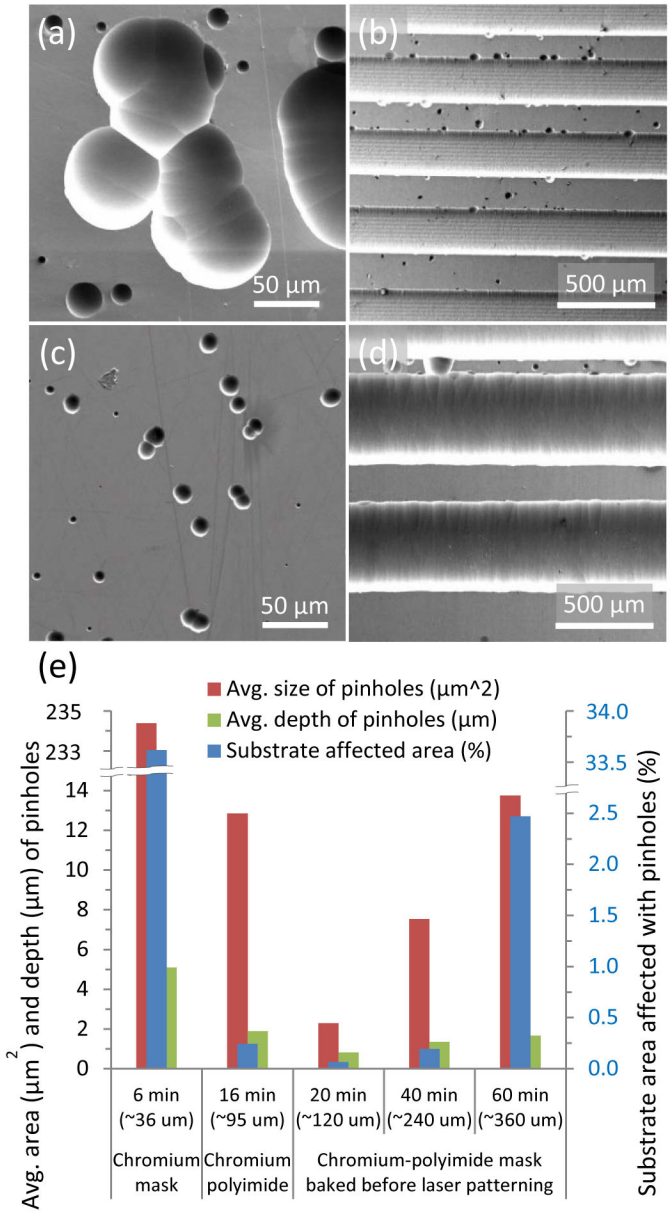

Figure 8.

Mask pinhole defects. (a, b) Chromium metal mask; after 6 min. in HF acid. (c, d) Chromium-polyimide baked mask; after 60 min. in HF acid. (e) Characterization of the mask quality with respect to pinhole defects for three mask types in terms of the average area and depth of the pinhole defects, and fraction of affected substrate area.